

The morphological characterization of the forewing of the *Manduca sexta* species for the application of biomimetic flapping wing micro air vehicles

This article has been downloaded from IOPscience. Please scroll down to see the full text article.

2012 Bioinspir. Biomim. 7 046011

(<http://iopscience.iop.org/1748-3190/7/4/046011>)

View [the table of contents for this issue](#), or go to the [journal homepage](#) for more

Download details:

IP Address: 131.84.11.215

The article was downloaded on 01/11/2012 at 16:01

Please note that [terms and conditions apply](#).

Report Documentation Page

Form Approved
OMB No. 0704-0188

Public reporting burden for the collection of information is estimated to average 1 hour per response, including the time for reviewing instructions, searching existing data sources, gathering and maintaining the data needed, and completing and reviewing the collection of information. Send comments regarding this burden estimate or any other aspect of this collection of information, including suggestions for reducing this burden, to Washington Headquarters Services, Directorate for Information Operations and Reports, 1215 Jefferson Davis Highway, Suite 1204, Arlington VA 22202-4302. Respondents should be aware that notwithstanding any other provision of law, no person shall be subject to a penalty for failing to comply with a collection of information if it does not display a currently valid OMB control number.

1. REPORT DATE 23 OCT 2012	2. REPORT TYPE	3. DATES COVERED 00-00-2012 to 00-00-2012	
4. TITLE AND SUBTITLE The morphological characterization of the forewing of the Manduca sexta species for the application of biomimetic flapping wing micro air vehicles		5a. CONTRACT NUMBER	
		5b. GRANT NUMBER	
		5c. PROGRAM ELEMENT NUMBER	
6. AUTHOR(S)		5d. PROJECT NUMBER	
		5e. TASK NUMBER	
		5f. WORK UNIT NUMBER	
7. PERFORMING ORGANIZATION NAME(S) AND ADDRESS(ES) Air Force Institute of Technology/ENY, Department of Aeronautics and Astronautics, 2950 Hobson Way, Wright-Patterson AFB, OH, 45458		8. PERFORMING ORGANIZATION REPORT NUMBER	
9. SPONSORING/MONITORING AGENCY NAME(S) AND ADDRESS(ES)		10. SPONSOR/MONITOR'S ACRONYM(S)	
		11. SPONSOR/MONITOR'S REPORT NUMBER(S)	
12. DISTRIBUTION/AVAILABILITY STATEMENT Approved for public release; distribution unlimited			
13. SUPPLEMENTARY NOTES			
14. ABSTRACT To properly model the structural dynamics of the forewing of the Manduca sexta species, it is critical that the material and structural properties of the biological specimen be understood. This paper presents the results of a morphological study that has been conducted to identify the material and structural properties of a sample of male and female Manduca sexta specimens. The average mass, area, shape, size and camber of the wing were evaluated using novel measurement techniques. Further emphasis is placed on studying the critical substructures of the wing: venation and membrane. The venation cross section is measured using detailed pathological techniques over the entire venation of the wing. The elastic modulus of the leading edge veins is experimentally determined using advanced non-contact structural dynamic techniques. The membrane elastic modulus is randomly sampled over the entire wing to determine global material properties for the membrane using nanoindentation. The data gathered from this morphological study form the basis for the replication of future finite element structural models and engineered biomimetic wings for use with flapping wing micro air vehicles.			
15. SUBJECT TERMS			
16. SECURITY CLASSIFICATION OF:			17. LIMITATION OF ABSTRACT
a. REPORT unclassified	b. ABSTRACT unclassified	c. THIS PAGE unclassified	Same as Report (SAR)
			18. NUMBER OF PAGES 14
			19a. NAME OF RESPONSIBLE PERSON

The morphological characterization of the forewing of the *Manduca sexta* species for the application of biomimetic flapping wing micro air vehicles

R P O'Hara and A N Palazotto

Department of Aeronautics and Astronautics, Air Force Institute of Technology/ENY, 2950 Hobson Way, Wright-Patterson AFB, OH 45458, USA

E-mail: ryan.ohara@afit.edu and anthony.palazotto@afit.edu

Received 11 April 2012

Accepted for publication 8 August 2012

Published 23 October 2012

Online at stacks.iop.org/BB/7/046011

Abstract

To properly model the structural dynamics of the forewing of the *Manduca sexta* species, it is critical that the material and structural properties of the biological specimen be understood. This paper presents the results of a morphological study that has been conducted to identify the material and structural properties of a sample of male and female *Manduca sexta* specimens. The average mass, area, shape, size and camber of the wing were evaluated using novel measurement techniques. Further emphasis is placed on studying the critical substructures of the wing: venation and membrane. The venation cross section is measured using detailed pathological techniques over the entire venation of the wing. The elastic modulus of the leading edge veins is experimentally determined using advanced non-contact structural dynamic techniques. The membrane elastic modulus is randomly sampled over the entire wing to determine global material properties for the membrane using nanoindentation. The data gathered from this morphological study form the basis for the replication of future finite element structural models and engineered biomimetic wings for use with flapping wing micro air vehicles.

(Some figures may appear in colour only in the online journal)

1. Introduction

The *Manduca sexta* species of moth, figure 1, serves as a source of biological inspiration for the future of micro air vehicle flapping flight. *Manduca sexta*, commonly referred to as the tobacco hawkmoth, is a moth of the family Sphingidae and is indigenous to North America. During their larval stage they are commonly referred to as hornworms. These hornworms primarily feed on tobacco and tomato plants, but will occasionally feed on potato and pepper crops and other plants in the Solanaceae family, hence their name *Manduca*, which is the Latin word for 'glutton'. Adults are large moths

with long forewings and small hindwings and are generalist nectar feeders.

They are strong fliers that have highly flexible wings that reverse camber and allow them to hover, with a rapid wing beat and are sometimes mistaken for hummingbirds [4, 12]. Characteristic flight parameters are detailed in table 1. Further, *Manduca sexta* has the ability to continue to fly and hover when its hindwings have been removed [9]. *Manduca sexta* are readily studied because they are easily reared in a laboratory, have short life cycles and their large size allows for many diverse scientific investigations on their various biological systems. Research topics include: flight mechanisms, nicotine resistance, hormonal regulation and hemolymph physiology



Figure 1. *Manduca sexta* specimen.

Table 1. Average parameters of *Manduca sexta* flight kinematics [3, 23].

Parameter	Range
Wing beat frequency	24.8–26.5 Hz
Hovering stroke amplitude	115°–120°
Forward flight stroke amplitude	100°–105°

Table 2. *Manduca sexta* and primary subcomponents.

1	Forewing—left
2	Forewing—right
3	Hindwing—left
4	Hindwing—right
5	Head
6	Thorax
7	Abdomen

Male and female specimens are received as pupae and placed into an incubator. After a period of several days, ecdysis occurs, and the adult specimen emerges from its pupal case. After a period of two to three days, to allow the moths wings to fully harden, the specimen is harvested for further study [12].

[17]. The compilation of these capabilities make the forewing of this species a great candidate for future study and application of biomimetic research toward FWMAVs.

2. Morphological study

To date a detailed study, with accompanying data, has not been conducted on the *Manduca* species that is sufficient enough to generate a representative structural dynamics model of the *Manduca sexta* forewing. To properly understand the structural dynamics of the forewing of the *Manduca sexta*, it is important to properly understand the context of the structural properties of the system to which this wing belongs. In order to fill this gap, a detailed morphological study of key features of numerous *Manduca sexta* specimens is presented here.

2.1. Mass and area measurement techniques

When a moth is ready for study, the entire moth is weighed and a top down image of the specimen is taken, figure 1. The specimen is then dissected into seven component pieces, table 2.

Each of these pieces is then placed on a green colored background with a reference marker and photographed with a digital camera as shown in figure 2. Using common image analysis techniques, the pixel by pixel area of each of the component pieces can be analyzed [16]. Using the image processing toolboxes available through Matlab, the image background is removed, translated into grayscale, and thresholded to black and white. Small objects are removed, and the remaining boundaries of the moth subcomponents are traced. Using a reference marker of a known shape and size, the

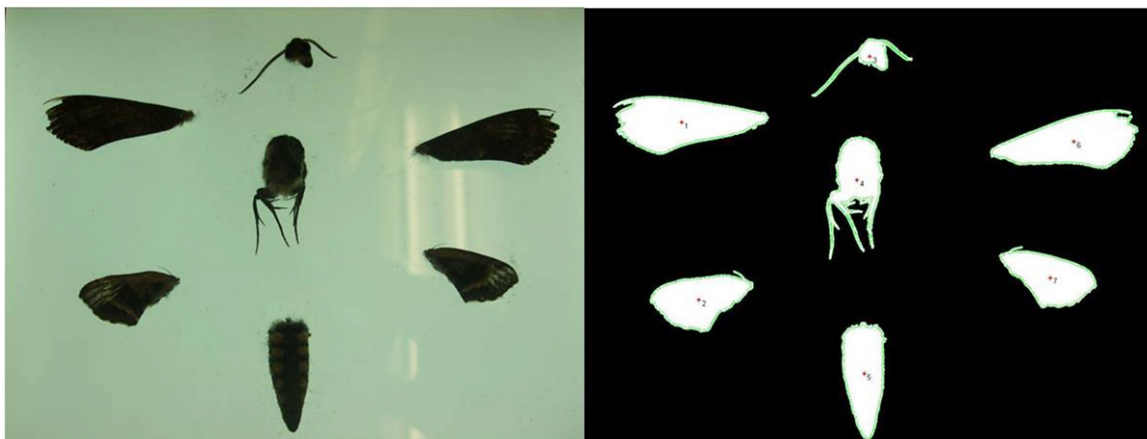


Figure 2. *Manduca sexta* component raw and threshold images.

Table 3. *Manduca sexta* mass properties.

SAMPLE	MOTH (g)	FW LT (g)	FW RT (g)	HW LT (g)	HW RT (g)	HEAD (g)	THO (g)	ABD (g)	Total (g)	Diff (g)
AVG	1.553 04	0.034 66	0.035 76	0.012 17	0.012 20	0.105 74	0.583 96	0.721 67	1.506 15	0.046 89
STD	0.507 59	0.007 67	0.007 47	0.002 86	0.003 11	0.019 39	0.148 61	0.320 59	0.483 36	0.046 58
MAX	2.701 60	0.052 10	0.049 40	0.019 60	0.017 60	0.137 70	0.917 90	1.597 60	2.582 20	0.141 41
MIN	0.768 70	0.018 60	0.019 90	0.007 80	0.007 00	0.058 50	0.268 30	0.297 60	0.754 00	-0.001 00
% Total		2.23%	2.30%	0.78%	0.79%	6.81%	37.60%	46.47%	96.98%	3.02%

pixel information can be translated to physical measurement units. Depending on the sub-component, the length, width, area and approximate volume can be determined. Each of the component pieces are then individually weighed with a very precise digital scale, Ohaus Voyager Pro (VP214CN), that is calibrated to measure repeatably to 0.1 mg. The total processing time of mass and area measurements is completed in less than 10 min for each specimen.

2.2. Mass properties

Mass properties for 30 different specimens are presented in summary in table 3 and in detail in table A1—appendix A. The table lists the measured values for the moth and each subcomponent. The mass of the subcomponents relative to the weight of the entire insect is shown as a percentage. This latter value could prove to be useful to FWMAV design engineers in determining the design space for their application. This testing revealed that the average weight of a single specimen is $1.55 \pm .050$ g. The weight of the forewings averages to 34.6 mg and represents 2.23% of the total mass of the insect. The hindwings weigh, on average, 12 mg and make up 0.78% of the total mass. The head, which could be akin to the control system, weighs approximately 105.6 mg and represents 6.81% of the mass of the moth. The thorax, which is the primary drive mechanism for flight, weighs approximately 58.3 mg and represent 37.6% of the total mass. Finally, the abdomen, which performs power generation and energy storage in addition to carrying the primary payload of the moth (eggs), typically weighs 72.1 mg and represents approximately 46.47% of the mass of the moth. As a check, the sum of the component measurements is presented and indicates that there is a 3% loss of mass from the first measurement of the entire specimen. These small differences are attributed to handling of the specimen and possible loss of very small pieces of the specimen during the dissection process.

An additional study was carried out to determine the mass contribution of the scales that are indicative to the wings of this species. This study was performed by liberating the forewings of the *Manduca sexta* as previously described. This process was performed as gently as possible to prevent the removal of any of the scales during the liberation process. The wings were immediately weighed and their masses recorded. Following this, the scales were carefully removed, using a bristled brush, that had been slightly dampened with water to prevent the aerial dispersal of the scales. Upon removal of the wing scales, the wings were then weighed again. The time for this process

Table 4. *Manduca sexta* scale mass.

Sample	Wing w/scales (g)	Wing w/out scales (g)	Difference (g)	Scale percentage –
AVG	0.0296	0.0233	0.0063	20.6%
STD	0.0064	0.0040	0.0030	5.4%
MAX	0.0401	0.0291	0.0118	31.2%
MIN	0.0197	0.0162	0.0035	13.5%

was on the order of 3–5 min, eliminating the possible loss of mass to desiccation. Due to the hydrophobic nature of the scales and the membrane, as evidenced by the beading of water on these surfaces, it is felt that there is no mass contribution to the use of water and a bristled brush to remove the scales. This was confirmed by rewetting the wing membrane after measurement, lightly drying the membrane with a paper cloth and remeasuring the wing. Differences in mass were less than 0.5 mg of the first membrane only measurement. The results of this study are presented in summary in table 4 and in detail in table B1—appendix B. This testing has revealed that for the forewing of the *Manduca sexta* species, the scales of the forewing represent, on average, 20.6% of the forewing mass. This is a significant amount of mass and is considerably larger than amounts previously reported in more general studies of a number of different species of insects [4].

2.3. Forewing area properties

Using the methods described above, 24 individual forewings, both left and right, were measured to determine their basic shape. A summary of the results of this analysis are presented in table 5 and in detail in table C1—appendix C. The wing shape is described by a number of common features related to the geometry of the wing. The wing length is represented by R and is typically found to be roughly 45–55 mm in length. The wing area S is typically found to be 715 mm^2 . It is more useful to express the wing area in terms of the wing length, R , and aspect ratio, AR , which is equal to the span, $2R$, divided by the mean chord, $S/2R$, where $AR = 4R^2/S$ [21]. Aspect ratios of the forewing of *Manduca sexta* fall in the 14.0–15.0 range. The area centroid is computed and falls at roughly 37.3% of the wing length and at 59.5% of the maximum wing chord.

Table 5. *Manduca sexta* forewing area properties.

	AR	S (mm ²)	CentroidX (mm)	CentroidX % Length	CentroidY (mm)	CentroidY % Chord	Length R (mm)	Chord C (mm)
AVG	14.42	702.46	18.61	37.3%	14.046	59.5%	50.18	22.97
STD	0.44	99.20	7.65	15.5%	5.164	10.8%	3.53	5.31
MAX	15.46	896.06	29.89	56.9%	20.708	78.4%	57.85	32.83
MIN	13.82	514.00	8.61	18.2%	7.607	45.1%	42.59	16.64

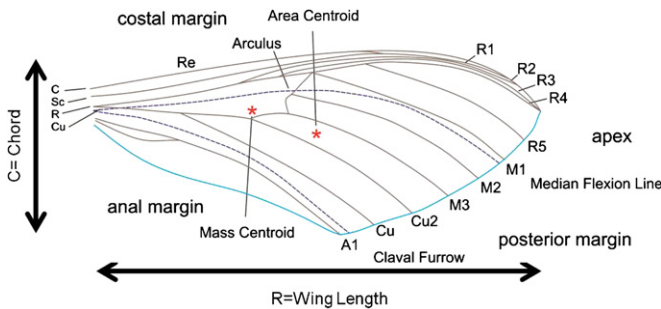


Figure 3. Venation map of *Manduca sexta* forewing [11].

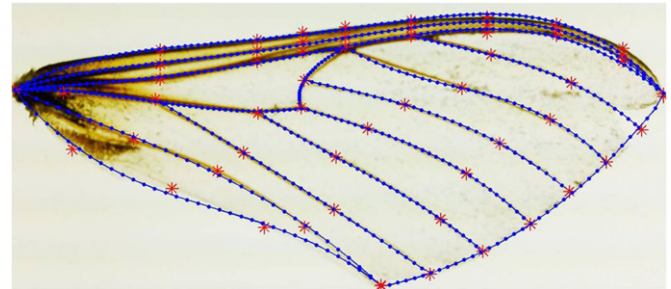


Figure 4. Splined wing.

2.4. Venation

Insect wings are formed from a complex makeup of polymer based chains, Chitin, that forms the cuticle, which provides the strong exoskeleton of the body, limbs and wings, acts as a barrier between the living tissues of the insect and the environment. Cuticle can range from rigid and armor-like venation to thin and flexible as in the membrane of the wing [6]. A fully developed wing consists of membranous regions of epidermal bilayers supported by venation. Extracellular cuticle layers expressed dorsally and ventrally from the epidermis determine the structural characteristics of the wing membrane [4]. Wing veins are typically hollow and are elliptical in cross section. The veins serve not only as structural members, but also as conduits for nerves and hemolymph.

A venation map of the *Manduca sexta* forewing is presented in figure 3. The naming convention and descriptions of the mapping are based on the Comstock–Needham system [11]. This diagram indicates the median flexion line, a radial groove or region of increased flexibility along which the wing can deform and yield variable camber [1]. The claval furrow, a similar line of flexion, where longitudinal bending occurs between the posterior anal veins and the posterior margin is also indicated. Wing mass is dominated by the mass contributions of the venation, flattened epidermal cells called scales and the membrane. The epidermal cells are primarily used for coloration, but may subtly influence flow patterns and boundary layer structure over wings [4, 24].

There is significant understanding of chitin, the long-chain polymer, a derivative of glucose, that is the main component of the exoskeletons and wings of insects [22]. Due to the ability of the biological specimen to vary the bonding chains, assemblage of nanofibers and crystalline structure, the material properties of chitin can vary over a wide range. The elastic

modulus can vary from 1–10 gigapascals (GPa) over a large variety of flying insect species [22].

2.4.1. Optical venation pattern detection. When initially viewed, the geometric structure of the hawkmoth wing can be seen as being very detailed and complex. However, after a period of study it can be found that there are actually many repeatable features in the wings themselves. Identification of the location of the main veins can be easily accomplished through graphical picking of a two-dimensional image. This image can be generated through any optical technique. All that is required is that the face of the imaging device be parallel to the surface of the wing to avoid any z-direction distortion. Scanning of the wing using an optical scanner is an excellent way to capture the required data. Removal of the scales from the wing is preferred to allow light to pass through the membrane to properly capture the location of the veins. The inclusion of a reference scale to allow for a known distance to pixel ratio calculation can also be helpful, but is not required.

Once the digital image of the wing is captured the leading edge vein can be identified by ten points at or near the root, 1/4 point, midpoint, 3/4 point, and tip. These points can be used with a fourth order polynomial curve fit to correctly identify the curvature of the leading edge vein. Remaining veins can also be described by four points at the root, midpoint and tip of the veins with a third order polynomial curve fit. With these equations in hand, 50–100 points are interpolated along each of these paths. The results of this graphical picking can be seen in figure 4. It can be clearly seen that all critical features and joint intersections have been properly located. This pattern detection will be used in section 2.4.2 to account for measurement error of the presented technique to determine the venation diameters of the wing.

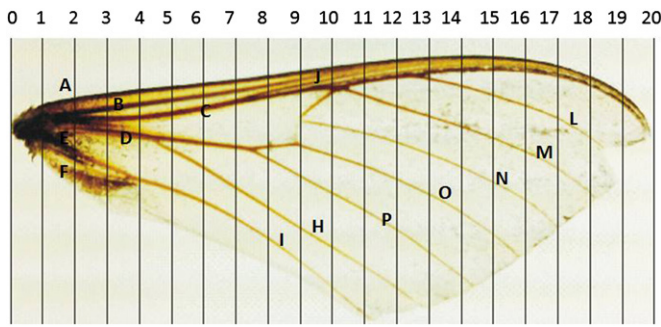


Figure 5. *Manduca sexta* forewing vein structure characterization.

2.4.2. *Venation cross section.* Previous research was performed using computed tomography to analyze the cross sectional area of the wing by looking at individual slices of CT data from the leading edge to the trailing edge of the wing [14]. Due to the small size of these veins, the CT imagery resolution of approximately 25 μm was not adequate to resolve the features along the length of the wing. A methodology for measuring the fine features of the venation using common pathological techniques was used to measure individual veins, with a resolution of less than 1 μm. The measurements from the presented techniques allow for a very accurate determination of the cross-sectional area of the vein compared with previous applied methods [19].

A study was carried out on five individual wings to determine the inner and outer diameters of the veins of the forewing of the *Manduca sexta* species. This was performed by placing the entire wing in a sectional mold of paraffin wax. As depicted in figure 5, sectional cuts were made from the root to the tip of the forewing at 2.5 mm intervals. The sectional cuts were then allowed to cool and then sliced using a microtome. They were either directly measured or dyed to allow easy visualization of the structure and then measured. Each of the sectional slices was then interrogated to determine two critical measurements of each of the veins in the sectional cut. Figure 6 depicts a sample result of the described process. Measurements of the outer and inner diameters of four veins from a sectional cut at 40% of the wing length are shown. The first vein, costal

(C), is located to the left of the wing, along the leading edge. The remaining subcostal (Sc) and radial (R1, R2) veins follow from left to right. It can be clearly seen that the veins are not circular, but rather elliptical in shape with large asymmetric fillet transitions [2, 26]. Using the previously defined optical measurements of the venation curvature, a correction of the diameter measurements based upon the oblique sectional cuts can be calculated. The data reported here include this corrected measurement for each wing. It is also of importance to note that the centroid of the veins is offset below the top surface of the membrane.

Figure 7 depicts the results of over 900 individual measurements of the outer and inner diameters of the five specimens. Each color in figure 7 represents the venation measurements of a single vein from the study. Due to the variability in the sizes of the wing samples, the measurements of the vein diameters were normalized by the diameter of the costal vein at the root of the wing. For all of the wing specimens, the outer and inner diameters of the veins linearly decline from root to tip as depicted by the dashed linear trend lines in figure 7 and equation (1). Y-values of equation (1) equal the calculated vein diameter and X-values refer to the percentage of the wing length.

$$\begin{array}{ll}
 \text{Mean outer diameter} & \text{Mean inner diameter} \\
 y(x) = p1 * x + p2 & y(x) = p1 * x + p2 \\
 p1 = -0.006056 & p1 = -0.00473 \\
 p2 = 0.7795 & p2 = 0.5896
 \end{array} \tag{1}$$

A linear relationship between the inner and outer vein diameters was also determined, equation (1). The inner diameter of the vein is on average within 73.2% of the vein outer diameter over the length of the wing. Maximum outer diameter measurements occur near the root of the wing along the leading edge, in the costal and radial veins. They typically range from 400–500 μm at these locations. Minimum outer vein measurements occur near the tip of the wing along the trailing edge in the anal veins. They typically range from 30–60 μm at these locations. It is far easier to measure the outer diameter of the veins using physical or optical measurement

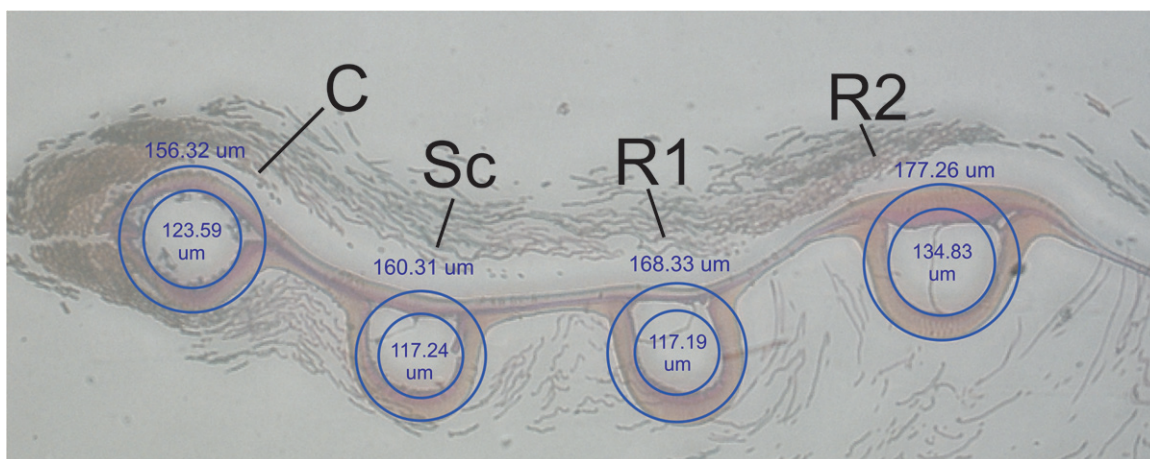


Figure 6. Vein pathology measurements: wing 1: 40% wing length (R).

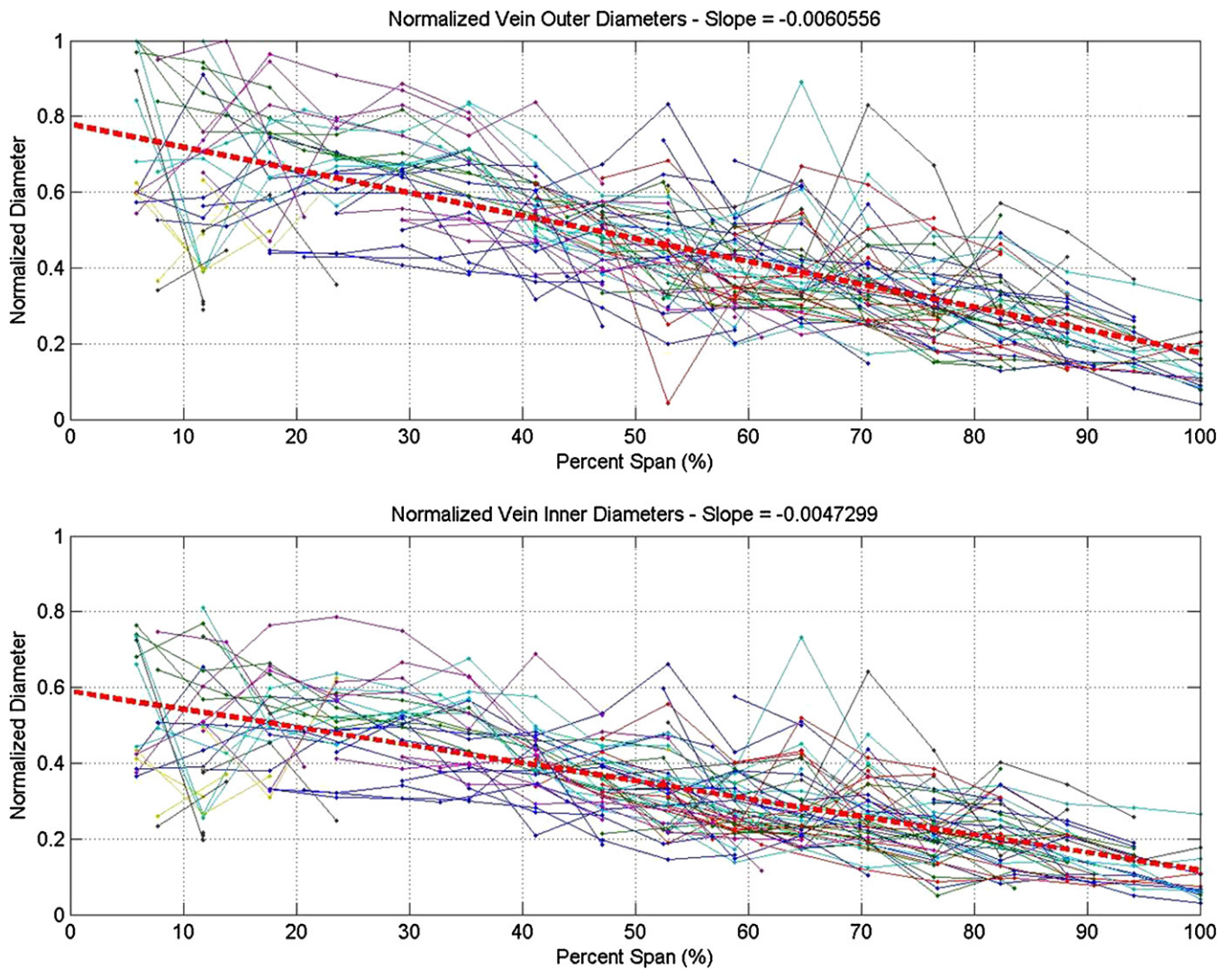


Figure 7. Normalized wing vein outer and inner diameters.

techniques. Through equation (1), the calculation of the interior features of the veins can be accounted for without directly taking these interior measurements and will aid in the determination of venation material properties in subsequent specimens.

2.4.3. *Venation elastic modulus.* The dynamic forced response of five costal and radial veins of the *Manduca sexta* are tested using simple cantilever beam conditions to predict the elastic modulus of the structure. The experimental forced response of the vein structure was tested using laser vibrometry and modal analysis. Through the use of previously discussed venation measurement technique, the outer diameter of the vein specimen can be physically measured and the subsequent volumetric structure of the wing can be analytically approximated using simple finite element analysis techniques. Using an unconstrained optimization technique, the unknown elastic modulus, E , of the vein structure can be easily approximated by tuning the analytical model to match the experimental results. This methodology has been used to

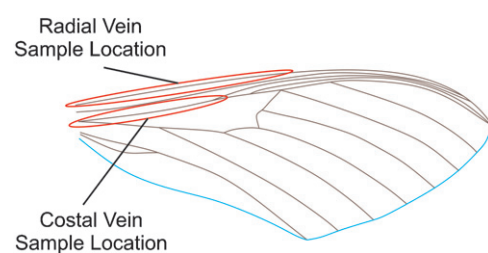


Figure 8. Radial and costal vein harvest locations.

successfully determine the material properties of composite plates and is applied here [8].

The experimental sample is harvested from a wing in which the membrane scales have been removed. Then a section of the leading edge radial vein or the costal vein is harvested from the wing as shown in figure 8. The membrane is closely trimmed to isolate the vein. The vein is then placed into a small clamping device that is lined with a medium density foam. This foam lined clamps allows the vein structure to be held, but not

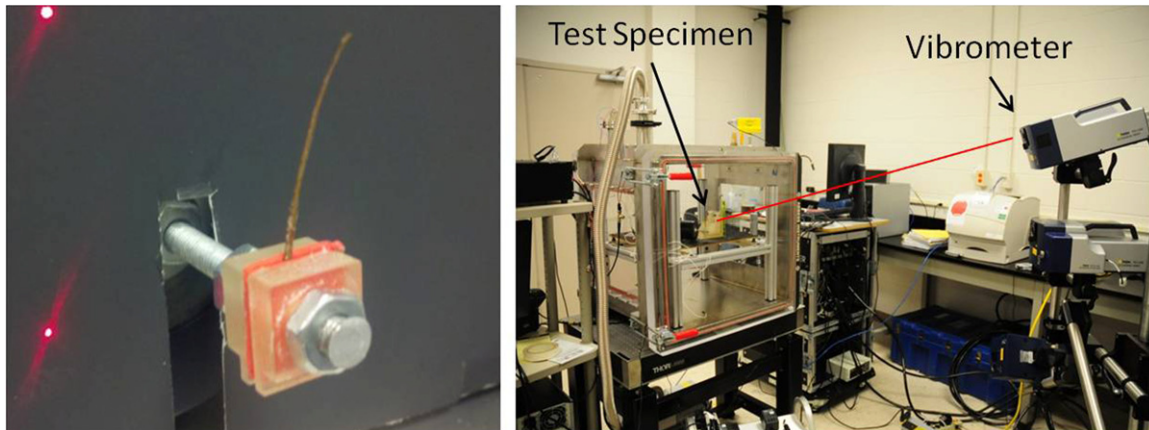


Figure 9. Experimental modal analysis: radial vein and scanning laser vibrometer.

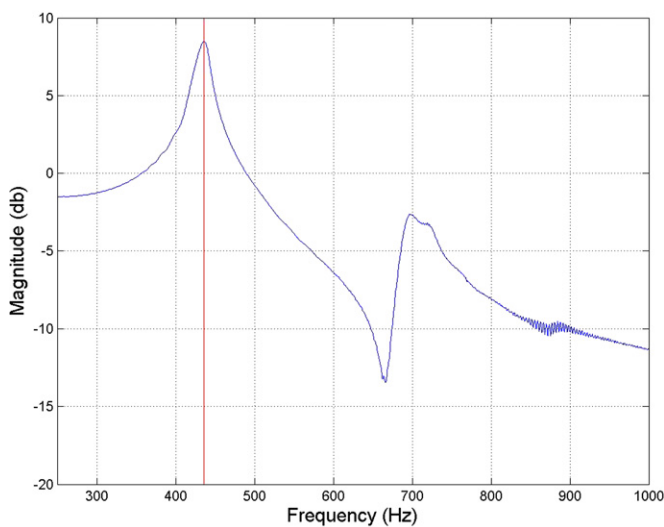


Figure 10. Experimental frequency response function at the vein tip.

crushed. The vein and clamping structure are then placed onto a piezo shaker that will provide the required base excitation required for modal analysis. In this case, the first eigenvalue of the vein structure is determined by experimentally determining the forced response of the vein, figure 9, through the use of a laser vibrometer and a pseudo random excitation. The results of this experimentation are shown in figure 10. The FEA model implements data from the venation cross sectional analysis to determine the inner diameter of the veins based on external measurements using both machinists calipers and optical measurements from a microscope. Volume is calculated during the FEA analysis and is coupled with a measurement of the mass of the vein to determine the density of the venation material.

With these data a one-hundred element tapered beam FEA model is generated to model the tested vein. Equation (2), depicts the simple cost function used to tune the fundamental frequency of the model to the experiment. By iterating on the elastic modulus variable of the FEA model, the minimization of J is realized as depicted in figure 11.

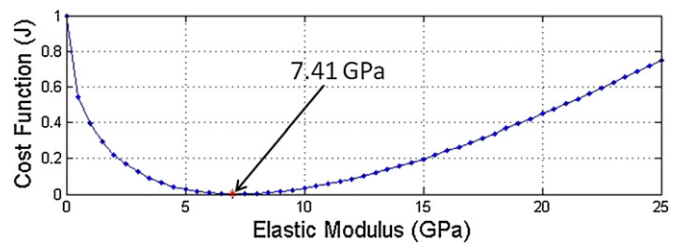


Figure 11. Cost function minimization.

Table 6. Experimental FEA input variable and venation elastic modulus results.

Vein location	Root OD (μm)	Tip OD (μm)	Length (μm)	Omega (Hz)	Density (g cm^3)	E (GPa)
Radial	500	476	15 724	518	2.6925	6.23
Costal	432	365	13 240	558	1.5152	7.82
Radial	418	391	14 472	470	2.3956	8.20
Radial	413	337	13 385	469	2.8963	7.63
Costal	432	320	15 153	436	2.6292	7.17
AVG	-	-	-	-	2.4258	7.41
STD	-	-	-	-	0.5394	0.75

$$J = \sum_{n=1}^{n_{\text{modes}}} \left[\left(\frac{\omega_{x,n}}{\omega_{f,n}} \right) - 1 \right]^2 \dots \omega_{x,n} = \text{EXP} \quad \omega_{f,n} = \text{FEA} \quad (2)$$

The results of this testing, as presented in table 6, show the mean elastic modulus to be 7.41 ± 0.75 GPa. This value lies within the range expected for similar flying species [19, 25].

2.5. Membrane

The membrane of the *Manduca sexta* forewing makes up the structural surface of the wing upon which the aerodynamic forces associated with flapping flight occur. The membrane serves to couple these aerodynamic forces with the structural venation of the wing. Understanding the material properties and shape of this surface is fundamental to the requisite

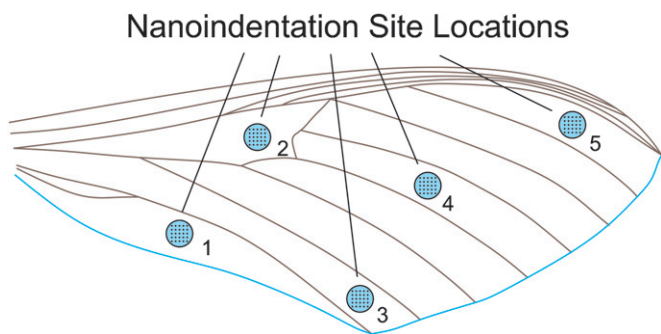


Figure 12. Nanoindentation site locations.

Table 7. Nanoindentation site location values.

Site	Site mean	Site STD
1	1.91	1.04
2	4.77	1.21
3	1.49	1.29
4	2.59	0.73
5	1.47	0.98
Global mean	2.45	–
Global STD	1.38	–

knowledge to properly understand the behavior of the *Manduca sexta* forewing.

2.5.1. Membrane material properties. The method of measuring hardness and elastic modulus by instrumented indentation is a common practice for determining the mechanical properties of thin films and small structural features [15]. The application of nanoindentation has been performed to determine the mechanical properties of the membranes of cicadas [19] and the tergal plate of *Manduca sexta* [7].

Nanoindentation was conducted using a MTS G200 nanoindenter on a single wing using membrane sections that had been isolated from the forewing of the *Manduca sexta*, figure 13. These membrane samples were processed by removal of the membrane’s scales and mounted on a glass slide through the application of a thin layer of cyanoacrylate adhesive. This glass slide had been previously mounted

on an aluminum puck using a Crystal Bond adhesive and allowed for easy mounting into the specimen carriage of the nanoindenter. Nanoindentations were made on a 5 × 5 grid, with 25 μm spacing, at a depth of 500 nm into the membrane surface, at random locations of the wing specimen as shown in figure 12. Approximately 20 min was required to process nanoindentations at each site. The total testing time of approximately 100 minutes is well within the 180 min window in which the wing has been shown to significantly desiccate [20]. Care was taken to ensure that all nanoindentation samples were taken over a homogeneous area of the wing membrane and not over the follicle of a wing scale. The surface of these membranes is presented in figure 14. The 25 indentation samples from each site location were then averaged to determine the local mean modulus over the particular measurement area. The local modulus values were then averaged to determine the global mean elastic modulus of the specimen, which was found to 2.446 ± 1.37 GPa. Both the local site modulus and global membrane modulus are presented in table 7. These results are consistent with other

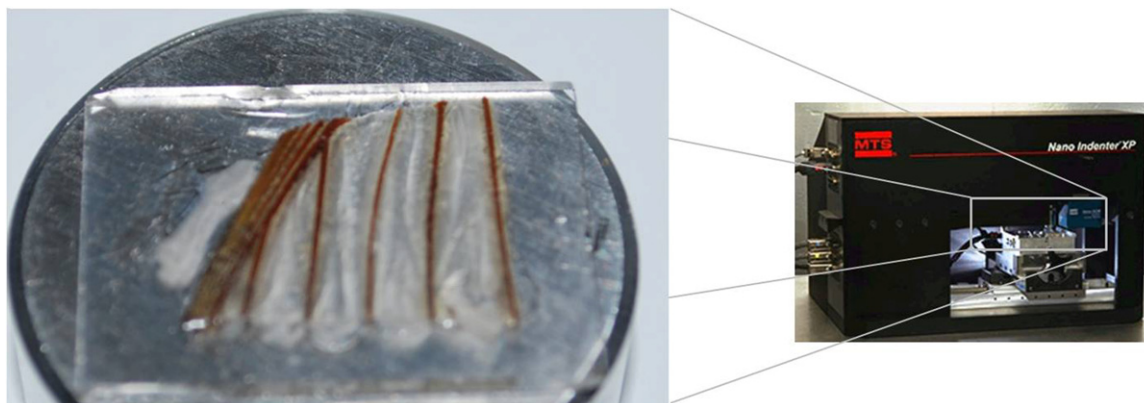


Figure 13. Membrane specimen mounted for testing in MTS nanoindenter.



Figure 14. Membrane surface without scales: 5×, 10×, 20×, 50×.



Figure 15. Alignment jig with wing unclamped and wing clamped.



Figure 16. Faro laser line scanner actively scanning wing.

species and fall within the range of similar species of winged insects [4, 19].

2.6. Wing camber

The forewing of the *Manduca sexta* species is a complicated three dimensional structure. In addition to the planar properties of span, chord, planform area and aspect ratio, it is important to quantify the shape of the wing. This three dimensional shape is quantified by the mean camber line of the wing. This camber is very important in determining the structural response and aerodynamic performance [4, 18]. Since the wing of the *Manduca sexta* species is so thin, the camber line represents its camber. Using a 3D coordinate measurement arm and laser line scanning system, it is possible to measure the camber of both engineered and biological wing profiles [10, 13]. Due to the variability of the size, shape and orientation of the forewings of the *Manduca sexta*, a methodology to measure the camber of the wings is presented that closely preserves the shape of the wing while it is attached to the abdomen of the specimen. The measurements taken in this study are of freshly liberated forewings that are placed into a clamping jig with soft foam. When the wing is liberated from the host, a conscious effort to keep the axillary sclerites at the wing base intact is made. In doing so, the axillary sclerites serve as a mount

to hold the wings within the soft foam lining of the clamp without distorting the camber of the wing compared to when the wing is attached to the specimen. The scanning process is completed within 5 min after liberation. The jig, shown in figure 15, was designed to have special alignment features to allow for easy postprocessing of the camber measurements in a known reference frame. The wings themselves were scanned with a Faro platinum laser line scanner, figure 16, with $\pm 35 \mu\text{m}$ accuracy and a scan rate of over 45 200 points per second. For this study, five pairs (left and right), for a total of ten forewings were scanned. Due to the rapid acquisition of the laser scanning system, roughly 80 000 three dimensional points were captured for each wing.

After the surface of each wing was captured, the wings were post processed to allow for proper orientation and comparison to the other wing scans. Using a polynomial least squares surface fitting technique, a third order cubic polynomial was fitted to the data in both the X -axis and Y -axis and is represented as equation (3).

$$z(x, y) = p00 + p10 * x + p01 * y + p20 * x^2 + p11 * x * y + p02 * y^2 + p30 * x^3 + p21 * x^2 * y + p12 * x * y^2 + p03 * y^3 \quad (3)$$

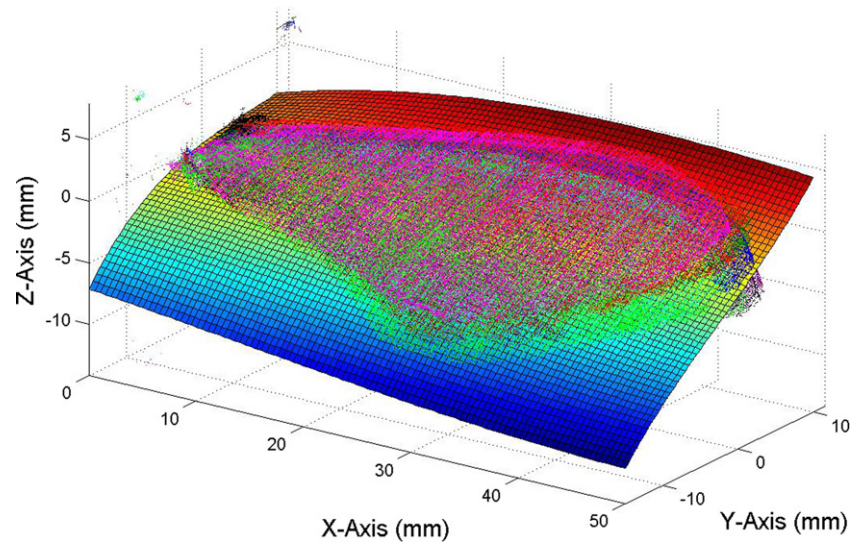


Figure 17. Point cloud data fitted with surface model.

$$\begin{aligned}
 p00 &= 0.1976 & p10 &= 0.07711 & p01 &= 0.1724 \\
 p11 &= 0.01626 & & & & \\
 p02 &= -0.01184 & p30 &= 0.00002401 & & (4) \\
 p12 &= 0.0003256 & p20 &= -0.003529 & & \\
 & & p21 &= -0.0001687 & p03 &= 0.00061
 \end{aligned}$$

Empirical testing found that this third order polynomial surface fit was the best compromise in terms of goodness of fit and overall representation of the camber of each wing. Additionally, the mean surface was calculated for all of the wings and the polynomial coefficients of this fit are presented in equation (4). The result of this surface fit as compared to the point clouds of each wing is presented in figure 17. With this three dimensional surface fit, the two dimensional data values of x and y can now be processed through the polynomial function in order to generate the z data required to properly model the camber for either an FEA structural model or for an equivalent engineered wing design. It is important to note that at the root of the wing the overall shape of the wing is concave up, and at the tip of the wing the shape is concave down. The transition between the two types of concavity occurs at 52% of the wing length. These shapes are much more complex than previous studies have realized and reflect the complex nature of this species [4, 5].

3. Conclusion

Through this detailed morphological study of the forewing of the *Manduca sexta* species, a better understanding of this species has been realized. Detailed study of the mass, area and volume properties of the moth and its subcomponents allows biologists and engineers to have a better understanding of the mass and size associated with these systems. This allows for the identification of the design space of a FWMAV

if this species of moth were to be used for the basis of a biomimetic design. Through the determination of the geometric properties of the venation and the surface of the wing, statistical models have been developed to determine these geometries along any per cent of the span of a wing. These models will aid in the future design of structural models and engineered wings that correctly reflect the geometry of this species. The determination of the material properties of the venation and the membrane coupled with these geometry models will allow for the calculation of the true stiffness of the wing. This calculated stiffness can then be used for the identification of engineered materials and the subsequent geometries necessary to fabricate wings with similar structural dynamics and aerodynamic characteristics to their biological counterpart. In conclusion, the authors found the amount of repeatability and linearity in the presented data to be very high. From mass and area calculations to venation diameters and material properties, all of the test results have been able to be repeated with small error bounds. Further, these errors can be minimized when considering the relative size of the individual sample and scaling the measurements according to the presented mean values. This conclusion allows the authors and other individual to step forward in the preparation of finite element models and derivative wing designs for FWMAVs with a high degree of confidence that was not previously available.

Acknowledgments

The authors would like to thank Dr Mark Willis and Jennifer Avondet from Case Western University, for the gracious support of this research. Through their aid, the *Manduca sexta* specimens for this study were obtained from their *Manduca sexta* colony. The authors also thank Dr Douglas Smith, AFOSR, for financial support of this research.

Appendix A

Table A1. *Manduca sexta* mass properties.

SAMPLE	MOTH (g)	FW LT (g)	FW RT (g)	HW LT (g)	HW RT (g)	HEAD (g)	THO (g)	ABD (g)	Total (g)	Diff (g)
1	1.3799	0.0324	0.0335	0.0091	0.0091	0.1128	0.5737	0.6017	1.3723	0.0076
2	1.0085	0.0290	0.0300	0.0100	0.0096	0.0671	0.3673	0.4854	0.9984	0.0101
3	0.7687	0.0222	0.0220	0.0078	0.0072	0.0585	0.2683	0.3680	0.7540	0.0147
4	1.6211	0.0327	0.0327	0.0089	0.0113	0.0969	0.6073	0.8101	1.5999	0.0212
5	1.4811	0.0270	0.0296	0.0105	0.0096	0.1056	0.5736	0.6634	1.4193	0.0618
6	1.3464	0.0274	0.0271	0.0102	0.0070	0.1032	0.6517	0.4830	1.3096	0.0368
7	1.9846	0.0412	0.0396	0.0141	0.0176	0.1129	0.7173	0.9687	1.9114	0.0732
8	2.2819	0.0425	0.0437	0.0196	0.0169	0.1313	0.8411	1.1139	2.2090	0.0729
9	2.4539	0.0521	0.0494	0.0176	0.0162	0.1348	0.8288	1.3025	2.4014	0.0525
10	1.5127	0.0396	0.0393	0.0125	0.0120	0.1139	0.6085	0.6478	1.4736	0.0391
11	1.4347	0.0383	0.0380	0.0109	0.0117	0.1084	0.5670	0.6499	1.4242	0.0105
12	1.6253	0.0383	0.0415	0.0130	0.0140	0.1264	0.6688	0.7174	1.6194	0.0059
13	1.0105	0.0273	0.0286	0.0109	0.0097	0.0870	0.3784	0.4667	1.0086	0.0019
14	1.0519	0.0322	0.0334	0.0135	0.0125	0.0894	0.4228	0.4375	1.0413	0.0106
15	0.9206	0.0295	0.0311	0.0100	0.0092	0.0807	0.4014	0.3456	0.9075	0.0131
16	1.0586	0.0339	0.0358	0.0109	0.0117	0.0961	0.4698	0.3938	1.0520	0.0066
17	1.0272	0.0330	0.0321	0.0108	0.0100	0.0958	0.4345	0.4112	1.0274	-0.0002
18	1.3285	0.0369	0.0406	0.0132	0.0136	0.1051	0.5181	0.5959	1.3234	0.0051
19	1.7663	0.0398	0.0469	0.0134	0.0151	0.1070	0.6526	0.7796	1.6544	0.1119
20	1.8652	0.0376	0.0412	0.0130	0.0133	0.1198	0.6599	0.9804	1.8652	0.0000
21	1.8261	0.0456	0.0388	0.0149	0.0152	0.1134	0.6598	0.8105	1.6982	0.1279
22	1.7800	0.0436	0.0473	0.0147	0.0147	0.1377	0.6085	0.8012	1.6677	0.1123
23	1.4826	0.0330	0.0358	0.0116	0.0116	0.1056	0.5233	0.6299	1.3508	0.1318
24	2.0363	0.0468	0.0458	0.0162	0.0163	0.1280	0.6865	0.9553	1.8949	0.1414
25	1.9020	0.0313	0.0326	0.0112	0.0112	0.1156	0.6020	1.0991	1.9030	-0.0010
26	1.3830	0.0277	0.0294	0.0090	0.0103	0.0999	0.5702	0.5606	1.3071	0.0759
27	2.7016	0.0349	0.0414	0.0145	0.0150	0.1324	0.7464	1.5976	2.5822	0.1194
28	0.9116	0.0186	0.0199	0.0096	0.0078	0.0842	0.4236	0.2976	0.8613	0.0503
29	1.1571	0.0245	0.0261	0.0080	0.0091	0.0866	0.5696	0.4153	1.1392	0.0179
30	2.4833	0.0408	0.0395	0.0154	0.0175	0.1162	0.9179	1.2606	2.4079	0.0754
AVG	1.553 04	0.034 66	0.035 76	0.012 17	0.012 20	0.105 74	0.583 96	0.72167	1.506 15	0.046 89
STD	0.507 59	0.007 67	0.007 47	0.002 86	0.003 11	0.019 39	0.148 61	0.32059	0.483 36	0.046 58
MAX	2.701 60	0.052 10	0.049 40	0.019 60	0.017 60	0.137 70	0.917 90	1.59760	2.582 20	0.141 41
MIN	0.768 70	0.018 60	0.019 90	0.007 80	0.007 00	0.058 50	0.268 30	0.29760	0.754 00	-0.001 00
% Total		2.23%	2.30%	0.78%	0.79%	6.81%	37.60%	46.47%	96.98%	3.02%

Appendix B

Table B1. *Manduca sexta* scale mass.

Sample	Wing w/scales (g)	Wing w/out scales (g)	Difference (g)	Scale percentage -
1	0.0401	0.0291	0.0110	27.4%
2	0.0308	0.0247	0.0061	19.8%
3	0.0277	0.0223	0.0054	19.5%
4	0.0318	0.0275	0.0043	13.5%
5	0.0378	0.0260	0.0118	31.2%
6	0.0197	0.0162	0.0035	17.8%
7	0.0258	0.0209	0.0049	19.0%
8	0.0285	0.0231	0.0054	18.9%
9	0.0244	0.0200	0.0044	18.0%
AVG	0.0296	0.0233	0.0063	20.6%
STD	0.0064	0.0040	0.0030	5.4%
MAX	0.0401	0.0291	0.0118	31.2%
MIN	0.0197	0.0162	0.0035	13.5%

Appendix C

Table C1. Forewing area properties.

	AR	S (mm ²)	CentroidX (mm)	CentroidX % Length	CentroidY (mm)	CentroidY % Chord	Length R (mm)	Chord C (mm)
1	13.88	687.30	24.18	49.5%	8.80	46.9%	48.84	18.76
2	13.82	655.39	22.19	46.6%	10.66	57.6%	47.58	18.52
3	15.21	647.32	23.87	48.1%	8.50	48.5%	49.61	17.53
4	13.98	750.80	25.36	49.5%	8.95	45.5%	51.22	19.67
5	15.24	585.32	22.69	48.1%	8.93	53.7%	47.22	16.64
6	14.11	653.75	23.06	48.0%	9.65	52.9%	48.03	18.24
7	14.05	815.72	9.74	18.2%	20.44	67.9%	53.52	30.10
8	14.47	675.42	10.21	20.7%	18.29	67.8%	49.42	26.97
9	14.22	857.53	14.98	27.1%	20.58	72.0%	55.21	28.60
10	14.12	514.00	11.10	26.1%	16.25	70.5%	42.59	23.03
11	13.91	618.66	12.17	26.2%	18.24	74.6%	46.38	24.46
12	14.61	789.97	10.39	19.4%	19.58	67.7%	53.71	28.93
13	14.45	722.04	28.54	55.9%	9.54	50.3%	51.07	18.94
14	14.44	692.42	28.44	56.9%	8.58	46.0%	50.00	18.65
15	14.29	678.61	27.03	54.9%	9.56	51.8%	49.25	18.46
16	14.26	792.13	29.89	56.2%	9.44	47.3%	53.14	19.97
17	15.46	607.31	26.66	55.0%	7.61	45.1%	48.45	16.85
18	14.18	693.16	27.74	56.0%	9.43	50.4%	49.57	18.71
19	14.40	838.82	12.96	23.6%	20.59	65.0%	54.95	31.66
20	14.43	683.12	11.86	23.9%	18.38	69.7%	49.65	26.38
21	14.94	896.06	12.61	21.8%	20.71	63.1%	57.85	32.83
22	14.88	523.22	8.61	19.5%	16.04	78.4%	44.12	20.47
23	14.37	690.97	11.20	22.5%	18.59	67.4%	49.83	27.56
24	14.30	789.96	11.16	21.0%	19.77	67.6%	53.14	29.25
AVG	14.42	702.46	18.61	37.3%	14.046	59.5%	50.18	22.97
STD	0.44	99.20	7.65	15.5%	5.164	10.8%	3.53	5.31
MAX	15.46	896.06	29.89	56.9%	20.708	78.4%	57.85	32.83
MIN	13.82	514.00	8.61	18.2%	7.607	45.1%	42.59	16.64

References

- [1] Combes S A 2010 Materials, structure, and dynamics of insect wings as bioinspiration for MAVs *Encyclopedia Aerospace Eng.* (Hoboken, NJ: Wiley)
- [2] Combes S A and Daniel T L 2003 Flexural stiffness in insect wings II. Spatial distribution and dynamic wing bending *J. Exp. Biol.* **206** 2989–97
- [3] DeLeon N E and Palazotto A N 2011 The evaluation of a biologically inspired engineered MAV wing compared to the *Manduca sexta* wing under simulated flapping conditions *Int. J. Micro Air Vehicles* **3** 149–68
- [4] Dudley R 1999 *The Biomechanics of Insect Flight: Form, Function, Evolution* (Princeton, NJ: Princeton University Press)
- [5] Ennos A R 1988 The importance of torsion in the design of insect wings *J. Exp. Biol.* **140** 137–60
- [6] Gullan P J and Cranston P S 2005 *The Insects: An Outline of Entomology* 3rd edn (Malden, MA: Blackwell)
- [7] Hollenbeck A C and Palazotto A N 2012 Methods used to evaluate the hawkmoth (*Manduca sexta*) as a flapping-wing micro air vehicle *Int. J. Micro Air Vehicles* **4** 119–32
- [8] Hwang S and Chang C S 2000 Determination of elastic constants of materials by vibration testing *Compos. Struct.* **49** 183–90
- [9] Jantzen B and Eisner T 2008 Hindwings are unnecessary for flight but essential for execution of normal evasive flight in Lepidoptera *Proc. Natl Acad. Sci. USA* **105** 16636–40
- [10] Liu T, Kuykendoll K, Rhew R and Jones S 2004 Avian wings *24th AIAA Aerodynamic Measurement Technology and Ground Testing Conf.*
- [11] Meyer J R 2007 External anatomy: wings www.cals.ncsu.edu/course/ent425/tutorial/wings.html
- [12] Norris A, Palazotto A and Cobb R 2010 Structural dynamic characterization of and insect wing: toward the development of bug sized flapping wing micro air vehicles *American Institute of Aeronautics and Astronautics AIAA-2010-2790*
- [13] O'Hara R P and Brown J M 2004 Experimental investigation of geometric uncertainty effects on blade forced response *40th AIAA/ASME/SAE/ASEE Joint Propulsion Conf. and Exhibit (Fort Lauderdale, FL)*
- [14] O'Hara R P, DeLeon N and Palazotto A 2011 Structural identification and simulation of the *Manduca sexta* forewing *SDM Conf. (Denver, CO)*
- [15] Oliver W C and Pharr G M 2003 Measurement of hardness and elastic modulus by instrumented indentation: advances in understanding and refinements to methodology *J. Mater. Res.* **19** 3–20
- [16] Pratt W K 2001 *Digital Image Processing* (Hoboken, NJ: Wiley)
- [17] Richman D 2011 Tobacco hornworm <http://entomology.unl.edu/k12/caterpillars/hornworm/hornwormpage.html>
- [18] Sims T 2010 A structural dynamic analysis of a *Manduca sexta* forewing *Master's Thesis* Air Force Institute of Technology, Wright-Patterson AFB, OH
- [19] Song F, Lee K L, Soh A K, Zhu F and Bai Y L 2004 Experimental studies of the material properties of the forewing of cicada *J. Exp. Biol.* **207** 3035–42
- [20] Tubbs T 2011 Biological investigation of the stimulated flapping motions of the moth, *Manduca sexta* *Master's Thesis* Air Force Institute of Technology, Wright-Patterson AFB, OH

- [21] Usherwood J R and Ellington C P 2002 The aerodynamics of revolving wings I. Model hawkmoth wings *J. Exp. Biol.* **205** 1547–64
- [22] Vincent J F and Wegst U G 2004 Design and mechanical properties of insect cuticle *Arthropod Struct. Dev.* **33** 187–99
- [23] Willmott A P and Ellington C P 1997 The mechanics of flight in the hawkmoth *Manduca sexta*: I. Kinematics of hovering and forward flight *J. Exp. Biol.* **200** 2705–22
- [24] Wootton R J 1992 Functional morphology of insect wings *Annu. Rev. Entomol.* **37** 113–40
- [25] Wootton R J, Evans K E, Herber R and Smith C W 2000 The hind wing of the desert locust II. Mechanical properties and functioning of the membrane *J. Exp. Biol.* **203** 2933–43
- [26] Wootton R J, Evans K E, Herber R and Smith C W 2003 The hind wing of the desert locust III. A finite element analysis of a deployable structure *J. Exp. Biol.* **203** 2945–55